PERGAMON

International Journal of Heat and Mass Transfer 44 (2001) 3345–3357

International Journal of HEAT and MASS TRANSFER

www.elsevier.com/locate/ijhmt

Measurement of solute diffusivities. Part II. Experimental measurements in a convection-controlled shear cell. Interest of a uniform magnetic field

V. Botton *, P. Lehmann, R. Bolcato, R. Moreau, R. Haettel

Lab EPM-MADYLAM, ENSHMG, BP 95, 38402 St Martin d'Hères, France

Received 25 February 2000

Abstract

Measurements of impurity diffusion coefficients in liquid metals show an important scattering. As this coefficient is very small, even weak convection significantly enhances mass transport and leads to an overestimate of the measured coefficient. We propose here a measurement method using the braking effect of a uniform magnetic field in liquid metals and semiconductors. We used a shear cell, where both solutal and thermal convection are precisely controlled. Magnetic fields up to 0.75 T were applied during diffusion experiments with the Sn–SnIn(1%at.) and Sn–SnBi(0.5%at.) couples. The theoretical braking laws of convection were verified and values consistent with previous microgravity experiments were found. © 2001 Elsevier Science Ltd. All rights reserved.

1. Introduction: the misfortunes of impurity diffusion coefficient measurements

The knowledge of the impurity diffusion coefficient in liquid metals and semiconductors is of high interest for metallurgists and crystal growers, since this parameter governs several phenomena such as segregation in crystals or microstructures in casting (primary spacing, dendrite tip radius,...) [1]. Moreover, from a more fundamental point of view, the value of this coefficient – actually its dependence on temperature – gives some crucial information about the atomic structure of liquid metals. Thus, a large amount of measurements have been performed during the last century. The principle of such measurements is rather simple and has not basically changed since the end of the 19th century: two liquid metallic alloys of different compositions are put into contact at a given time and one lets diffusion proceed during a long enough period of time to allow a fairly good measurement of the concentration profile. A fit of the concentration profile measured after a chosen duration with a theoretical prediction gives the value of the impurity diffusion coefficient [2].

However, the value of this transport coefficient is still badly known [3]. This is due to its very low value, about 10^{-9} m^2 s^{-1}, which makes the experiments extremely sensitive to convective transport. Even a very low convective velocity (about 0.1 μm/s) is enough to change diffusive transport into convecto-diffusive transport, thus enhancing the transport and artificially increasing the measured value. This convection has mainly two origins. First, the two liquids put into contact have different densities; the density variation within the mixing zone yields (under normal gravity) solutal buoyancy forces. Secondly, any experiment with liquid metals is performed at so high temperatures (from 300°C to 2000°C) that it is very difficult to achieve a uniform temperature along a typically 20 cm long experiment. Even temperature differences on the order of 0.1°C are sufficient to force the experiment to fail. Several attempts to reduce this natural convection have been made. The most widely used technique is to perform vertical experiments, in order to stabilise the flow: the heaviest liquid is at the bottom and sometimes a vertical stabilising temperature gradient is applied. However, because of the vicinity of the thermal unit (furnace,

* Corresponding author. Tel.: +33-4-7682-5202.
E-mail address: valery.botton@hmg.inpg.fr (V. Botton).

0017-9310/01/$ - see front matter © 2001 Elsevier Science Ltd. All rights reserved.
PII: S0017-9310(00)00362-8

cooling device,...), small horizontal temperature gradients are unavoidable and Alexander et al. [4] have numerically shown that they may deeply modify the measured value. Another possibility is to reduce the diameter of the crucible in which the metal is contained, as the convective velocity increases at the diameter to the power fourth [5]. This approach has also shown its limits: in capillary tubes of diameters smaller than 1 mm, unexpected variations of the measured diffusion coefficient are observed. This has sometimes been interpreted by the so-called "wall-effect" or "second order Marangoni effect", due to the atomic contact between the liquid and the crucible [6]. However, it has been shown that the typical extent of such phenomena would not be greater than 50 Å from the boundary [7]. The main reason of this discrepancy may simply be the difficulty to properly fill a 0.8 mm capillary tube with a liquid metal, because of the problem of bad wetting and the presence of oxides. As a matter of fact, these measurements exhibit a strong scattering [3]. The measured values may differ by over one order of magnitude depending on the authors. Moreover, it is well known among experimentalists, that even when performing several times the same experiment on the same device, the scattering may be around 30%. Is this scattering due to uncontrolled thermal convection, to vibrational convection, to Marangoni convection due to defects of wetting in the crucible, or to still another unknown phenomenon? This point is still far from being understood.

Up to now, the best method to get rid of these convective effects is to perform experiments in microgravity where buoyancy forces become negligible. The values measured in this environment are looked upon as the most reliable. However, each experiment is expensive both in time and money and reproducibility can hardly be tested. In electrically conducting liquids, an alternative to microgravity is the use of a uniform magnetic field. It is well known that a magnetic field may efficiently damp out any kind of convective motion and the scaling laws of this damping are available [8]. But it has been pointed out that the magnetic field might also modify atomic mobility in the liquid metals. Experiments performed by Youdelis et al. [9] seemed initially to show such an effect. The observed effect could actually be due to a simple damping of the flow and the authors demonstrated themselves a couple of years later [10] that the effect of a magnetic field on the atomic mobility should be far weaker. Our purpose in this paper is to present an attempt for measuring impurity diffusion coefficients in a liquid metal using a uniform steady magnetic field.

The first step to achieve such measurements is to precisely estimate the influence of the fluid flow on the measured diffusion coefficient and the braking effect of the magnetic field. One of the main properties of magnetohydrodynamic (MHD) braking is that the flow is never fully stopped, since the damping force is proportional to the fluid velocity. The strategy is therefore to perform experiments with different values of the magnetic field, to compare the measured apparent diffusion coefficient with the predictions of a model based on MHD damped convection flow, to validate this model, and finally to derive a value for the real impurity diffusion coefficient from the extrapolation to the case of an infinite magnetic field. The theoretical model of the MHD damped flow is therefore one of the key ingredients of this methodology, but it may be considered as well known [8]. The other important ingredient, which is a significant part of this paper, is the development of a theoretical model for the influence of the fluid flow on the apparent diffusion coefficient. Together, these ingredients result in a relationship between the apparent diffusivity and the applied magnetic field. If this relationship is systematically in good agreement with the experimental data, we may conclude that *we only have braked residual convection and that no significant atomic modification of diffusion motion has occurred*. This theoretical aspect is also discussed in part I of this paper in the case of solutal convection [11]. Here, in Section 2 of this paper, we essentially recall the basic physical phenomena and show some analytical and numerical solutions in the case of combined thermal and solutal convection which occur most frequently in the experiments.

The second step is an assessment of these relationships based on the comparison of our predictions with a "convection-controlled" diffusion experiment. Previous authors have tried to minimise convection as much as possible, but with no real control on it. Here, on the contrary, some thermal or solutal convection is created, strong enough (but still very weak) to mask any other residual motion (vibrational convection, Marangoni convection, etc.), and precisely controlled. The magnetic field can then be applied and the braking effect checked. As a matter of fact, the magnetic field does ignore the origin of the flow and the damping is proportional to the velocity whatever the driving mechanism. Then the hierarchy between different components of the actual flow is maintained in the presence of the magnetic field: the imposed component of the convective flow remains dominant over the others even when it is braked. This makes a great difference with previous experiments, either in microgravity (only the buoyant flow is damped out, but not vibrational or Marangoni flow) or on ground in vertical capillary tubes stably stratified. As convection can now be accurately controlled, it becomes possible to state if the scattering mentioned previously is due to convection or not.

In Sections 3 and 4 of this paper, we present the experimental device and the results obtained on two different diffusion couples. They are then compared to the theoretical predictions and conclusions are drawn on

the potentialities of this methodology for diffusivity measurements.

2. Influence of thermo-solutal convection on the apparent diffusion coefficient

2.1. Studied configuration and basic averaged equations

The diffusion experiment is modelled by an infinitely long horizontal capillary tube of diameter H, submitted to a constant axial temperature gradient $\partial T/\partial x = \Delta T/L$ and to a vertical uniform magnetic field of induction B, as illustrated in Fig. 1. This type of buoyancy-driven MHD flow has been studied in details by Garandet et al. [12], Alboussière et al. [8] and Davoust et al. [13]. The initial concentration profile is a step of height ΔC_0 and when the experiment is stopped, the variations of concentration are smoothly distributed along an axial length $2L$. The aim of this approach is to describe the shape of this axial profile (and its evolution in time) under the effect of diffusion along with MHD-damped thermo-solutal convection. The basic idea of this study is to describe mass transfer in the capillary tube by a 1D diffusion equation for the cross-section-averaged concentration. Thus, the purpose of the theoretical calculations is to define locally an effective diffusion coefficient which accounts for the convective enhancement of the mixing process. As expected from the work of Barat and Garandet [23], the ratio between the convective and the diffusive mass transfer contributions scales as $Pe^2 = H^2W^2/D^2$, where W, H and D represent, respectively, a typical velocity, the diameter of the capillary and the diffusion coefficient.

Taylor's fundamental work [14] dealt with forced convection in a capillary tube (Poiseuille profile). He showed that the 1D diffusion model is valid at times much longer than the radial diffusion characteristic time. Maclean and Alboussière [11], in part I of this paper, express this time as H^2/D and show, in the case of a shear-cell experiment, that this is the only assumption necessary to derive a 1D model. Under this assumption, given a velocity field $\mathbf{u}(x,y,z,t)$ with a no net flux condition on the contour of the capillary, one can derive the expected 1D diffusion equation. The (dimensional) transport equation is indeed

$$\frac{\partial c}{\partial t} + \mathbf{u}\nabla c = D\Delta c, \tag{1}$$

where the concentration $c(x,y,z,t)$ can be split into two parts: its average over the cross-section, $c_0(x,t) = \langle c(x,y,z,t)\rangle$, plus its fluctuations in the section, $c_1(x,y,z,t) = c - c_0$. It is shown in part I that c_0 and c_1 verify:

$$\frac{\partial c_0}{\partial t} + \frac{\partial}{\partial x}\langle u_x c_1\rangle = D\frac{\partial^2 c_0}{\partial x^2} \tag{2}$$

and

$$u_x \frac{\partial c_0}{\partial x} = D\Delta_S c_1, \tag{3}$$

where Δ_S denotes the Laplacian operator in a cross-section. Given the longitudinal component of the velocity field, and the shape of the cross-section, one can solve Eq. (3) to express c_1 as a function of u_x and c_0. Let us denote $\Delta_S^{-1}(u_x)$ the solution of $\Delta_S(f) = u_x$ with $\partial f/\partial n = 0$ on the contour of the cross-section. Then Eq. (2) becomes,

$$\frac{\partial c_0}{\partial t} = \frac{\partial}{\partial x}\left[D\left(1 - \frac{\langle u_x \Delta_S^{-1}(u_x)\rangle}{D^2}\right)\frac{\partial c_0}{\partial x}\right], \tag{4}$$

where the effective diffusion coefficient can be identified as

$$D_{\text{eff}} = D\left(1 - \frac{\langle u_x \Delta_S^{-1}(u_x)\rangle}{D^2}\right). \tag{5}$$

In the present case, we are mainly interested in natural convection, which occurs within a shear-cell or a long-capillary experiment, and its damping by a magnetic field. The exact solution for an horizontal cavity submitted to a steady longitudinal temperature gradient and a vertical magnetic field can be found in [15]. In this particular case, one can notice that a global effective diffusion coefficient can be defined thanks to the steadiness of the flow (because of the low Prandtl number, the temperature gradient is negligibly modified by weak convection). The bulk velocity is indeed of the form $u_x = u(z)(Gr_T/Ha^2)$, where z corresponds to the magnetic field direction and $Gr_T = (g\beta_T \Delta T/LH^4)/\nu^2$ and $Ha = \sqrt{(\sigma/\rho\nu)}BH$ are, respectively, the Grashoff and the Hartmann numbers. Here σ, ν and ρ represent the electric conductivity, kinematic viscosity and density of the fluid, respectively; β_t and β_c are its thermal and solutal expansion coefficients (note that all the physical properties of the fluid are assumed independent of the composition, as we deal with dilute alloys). The effective diffusivity is then provided by Eq. (5):

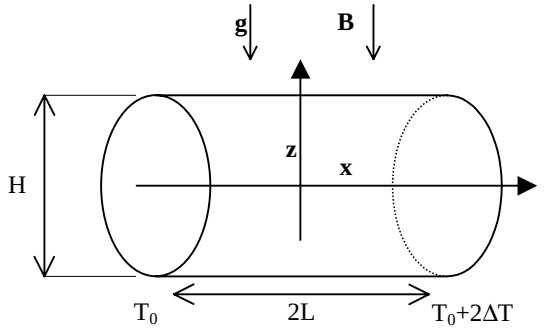

Fig. 1. Configuration of the EURIDICE experiments.

$$D_{\text{eff}} = D\left(1 + \frac{7}{384}\frac{Gr_T^2}{Ha^4}\right). \tag{6}$$

In the case of a shear-cell experiment, the initial concentration profile along the capillary is ideally a step function; thus a strong solutal convection occurs at least at the early stages of the experiment. The length on which concentration gradients spread evolves with time, thus the intensity of the flow is time-decreasing and no steady state is reached before the complete homogenisation of the mixture. Actually, the longitudinal velocity in the bulk can be written as:

$$u_x = u(z) \times \frac{Gr_S}{Ha^2}\frac{\partial c_0}{\partial x}(x,t), \tag{7}$$

where $Gr_S = (g\beta_S \Delta C_0 / LH^4)/\nu^2$ stands for the (constant) solutal Grashoff number. So the effective diffusion coefficient is space and time dependent and $D_{\text{eff}}(x,t) = f(x,t)(Gr_S^2/Ha^4)$, where f is some function of space and time. An analytical solution to the averaged concentration equation is provided in part I under the assumption of strong solute buoyancy-driven convection (i.e. neglecting both the axial molecular diffusion and thermal convection) with a vertical magnetic field. Our purpose is now to derive a general equation for combined solutal and thermal convection together with diffusion, as in any realistic experiment. An order of magnitude analysis then allows us to characterise the different possible experimental situations.

2.2. Asymptotic cases, scaling analysis and some experimental considerations

In order to solve Eq. (3), the first step is to express the longitudinal velocity $u(x,y,z,t)$ as a function of the averaged concentration $c_0(x,t)$. We assume the magnetic Reynolds number is very small, that inertia is much smaller than the electromagnetic damping force in the momentum equation (strong interaction parameter, $N = \sigma B^2 l/\rho u \gg 1$), and that the flow is steady, which holds after a time greater than the electromagnetic characteristic braking time $\sigma B^2/\rho \approx 10^{-4}$ s (see for example [16]). The Hartmann number is high, and only the bulk of the flow is first considered. That is to say both boundary layers and recirculating zones are ignored (the boundary layers contribution to the longitudinal mass transfer will be taken into account later). At last, the variation $c_1(x,y,z,t)$ of the concentration within a section is small compared to the averaged concentration $c_0(x,t)$. As shown by Maclean et al. [11], this assumption always holds when $t \gg H^2/D$.

The Navier–Stokes equation and Ohm's law are then

$$\frac{1}{\rho}\nabla p = \frac{1}{\rho}\mathbf{j} \times \mathbf{B} + [\beta_T(T - T_{\text{ref}}) + \beta_c(c - c_{\text{ref}})]g\mathbf{z}, \tag{8}$$

(in the frame of the Boussinesq approximation) and

$$\mathbf{j} = \sigma(-\nabla\phi + \mathbf{u} \times \mathbf{B}), \tag{9}$$

where T_{ref} and c_{ref} are references temperature and concentration taken in the centre of the capillary, ϕ is the electric potential and p is the pressure. The longitudinal component of velocity is found through analogy with the work of Cowley [17]. Its non-dimensional form is:

$$U(Z) = -2\left[\frac{Gr_T}{Ha^2} + \frac{Gr_S}{Ha^2}\frac{\partial C_0}{\partial X}(X,\tau)\right]Z, \tag{10}$$

where $Z = z/H$, $X = x/L$, $C = (c - c_{\text{ref}})/\Delta C_0$, $U = (H/\nu)u$, and $\tau = (D/L^2)t$. This profile is obviously the superposition of the thermal convection and solutal convection profiles. It is linear along the magnetic field lines. Eq. (4) can be written in non-dimensional form (using H as lateral length-scale and L as longitudinal length-scale and denoting Sc the Schmidt number):

$$\frac{\partial C_0}{\partial \tau} = \frac{\partial}{\partial X}\left[(1 - Sc^2\langle U\Delta_S^{-1}U\rangle)\frac{\partial C_0}{\partial X}\right]. \tag{11}$$

Considering a circular cross-section and the velocity field given by Eq. (10), the averaged term writes:

$$\langle U\Delta_S^{-1}U\rangle = -\frac{7}{384}\left[\frac{Gr_T}{Ha^2} + \frac{Gr_S}{Ha^2}\frac{\partial C_0}{\partial X}\right]^2. \tag{12}$$

It has been shown in Part I that, unless the Hartmann number reached values of several hundreds, the mass transfer through boundary layers and recirculations within the cross-section strongly affects the 7/384 coefficient in Eq. (12). We thus replace this value by an $\alpha(Ha)$ coefficient calculated numerically (see Fig. 3, Part I).

The 1D diffusion equation for the cross-section averaged concentration then writes:

$$\frac{\partial C_0}{\partial \tau} = \frac{\partial}{\partial X}\left\{\left[1 + \left(T + S\frac{\partial C_0}{\partial X}\right)^2\right]\frac{\partial C_0}{\partial X}\right\}, \tag{13}$$

denoting T and S the groups: $T = \sqrt{\alpha}(Gr_T Sc/Ha^2)$ and $S = \sqrt{\alpha}(Gr_S Sc/Ha^2)$. These parameters T and S represent the relative intensity of thermal and solutal convection compared to molecular diffusion. They are time independent. For $T = 0$ (no temperature gradient) one recovers the equation studied in part I. Notice that T is always positive while S can be positive if its contribution enhances the effect of thermal convection and negative if it opposes them. Care has to be taken that this last group, S, has been built using the longitudinal length-scale (L) at the end of the experiment. The actual order of magnitude of the solutal convective contribution is $S\Delta C_0/\Delta(\tau)$, where $\Delta(\tau)$ is the non-dimensional distance over which the variations of concentration spread at time τ. As already noticed, this order of magnitude may be very high for small values of τ. At last, let us recall that the two parameters S and T account for the elec-

tromagnetic braking of the flow in Ha^{-2}. Part I describes the temporal evolution of the concentration profile, for $t \gg H^2/D$, as a two phase process. The first phase is characterised by the domination of the solute buoyancy-driven convection; during this period, the $(1+T^2)$ term can be neglected in Eq. (13), which becomes:

$$\frac{\partial C_0}{\partial t} = 3S^2 \frac{\partial^2 C_0}{\partial X^2} \left(\frac{\partial C_0}{\partial X} \right)^2. \tag{14}$$

The mixing length Δ follows a $\tau^{1/4}$ evolution: $\Delta \sim S^{1/2}\tau^{1/4}$. Thus Eq. (14) is solved analytically in part I (expression 27, part I) providing a solution denoted here as the Maclean–Alboussière function. The second phase (where $(1+T^2)$ becomes predominant) is a constant effective diffusivity phase: neglecting the solutal terms in Eq. (13), one recovers:

$$\frac{\partial C_0}{\partial \tau} = (1+T^2) \frac{\partial^2 C_0}{\partial X^2}. \tag{15}$$

The temporal evolution is now of the form: $\Delta \sim (1+T^2)^{1/2}\tau^{1/2}$, and the well-known analytical solution is:

$$C_0 = 1/2 \operatorname{erf}\left(\frac{X}{2\sqrt{(1+T^2)\tau}} \right). \tag{16}$$

In the isothermal case, the date of the transition between these two phases was evaluated as $\tau_0 \sim S^2$ [11]. Keeping the thermal convection term in Eq. (13), a straightforward manipulation shows that the transition is reached at time $\tau_0 \sim S^2/(1+T^2)^2$.

From an experimental point of view, the measurement of the molecular diffusivity is easier when the second phase is reached. In such conditions, the effective diffusion coefficient is indeed constant in space and time; it writes $D_{\text{eff}} = (1+T^2)D$ and the correction term decreases as B^{-4} with the applied field. However, during the first solute-buoyancy driven phase, if we still analyse the concentration profile at time τ_m of the experiment as the product of a diffusive evolution, the apparent (global) coefficient is obtained by writing: $\Delta = (D_{\text{app}}\tau_m)^{1/2}$, with $\Delta \sim S^{1/2}\tau_m^{1/4}$. Thus $D_{\text{app}} = \Delta^2/\tau_m \sim S\tau_m^{-1/2}$, for $\tau_m \ll \tau_0$. The apparent diffusion coefficient follows then a B^{-2} law and is time-dependent. The date of the transition $\tau_0 \sim S^2/(1+T^2)^2$ between the B^{-2} and the B^{-4} regimes depends on the considered couple, on the temperature gradient and on the magnetic field. For a given couple and a fixed temperature gradient, the function $\tau_0(Ha)$ exhibits a maximum $\tau_{0\max} = [Gr_S/2Gr_T]^2$ for $Ha = \sqrt{\alpha Gr_T Sc}$ (this corresponds to $T=1$). This function is shown in Fig. 2 for SnIn(1%at.) and SnBi(0.5%at.), the couples which were tested experimentally. The vertical axis is graduated in non-dimensional time but an order of magnitude in hours is indicated. Although $\tau_{0\max}$ is of a few hours in the case of SnIn(1%), it is realistically not reachable in an experiment with SnBi under moderate magnetic field ($Ha < 100$), considering an experiment duration about 40 h. In principle, it would always be possible to reach the B^{-4} regime by increasing the temperature gradient (i.e. decreasing $\tau_{0\max}$). However, in practise, variations of the diffusion coefficient with temperature would not be negligible along the capillary. Thus, a B^{-4} evolution can be expected with the Sn–SnIn couple while a B^{-2} behaviour is observed on the Sn–SnBi couple in the present study.

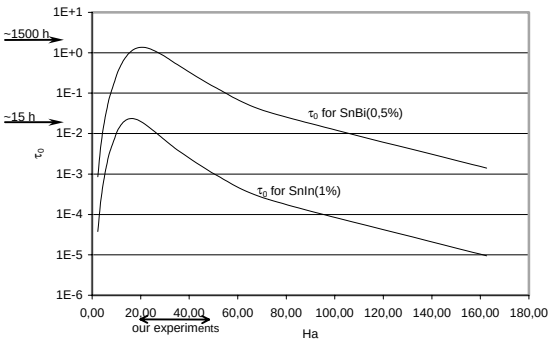

Fig. 2. Date of transition between the dominant buoyancy-driven convection phase and the 'constant effective diffusivity' phase.

3. The experimental device: a convection-controlled diffusion experiment

To perform our convection-controlled experiments, we used the now classical shear-cell technique [2,3] with some improvements to give a better control on the experiment (Fig. 3). The 210 mm long capillary tube is made up of 35 segments of inner diameter 2 mm. At the beginning, the cell's segments are aligned vertically and the two different alloys are melted in the reservoirs at the top of the experiment (diameter 6 mm, length 60 mm) as shown in Fig. 3(a), liquid A alternating with liquid B. It is thus possible to process four capillaries simultaneously. The upper segment is then moved to open the reservoirs and the capillaries are filled (Fig. 3(b)) under vacuum. After filling, the whole experiment is put under a slight overpressure of argon gas. The upper segment and the lower segment are then moved simultaneously to isolate the capillaries from the reservoirs (Fig. 3(c)). We thus trap two liquid elements at each end of the capillaries which will not contribute to the further diffusion process. These two pieces enable us, at the end of the experiment, to check that the composition of the initial liquids was uniform. The capillaries are then put horizontally in the magnet and half of the segments is turned 90°. Thus, liquid A comes in to contact with liquid B, liquid B with liquid A, and diffusion proceeds (Fig. 3(d)).

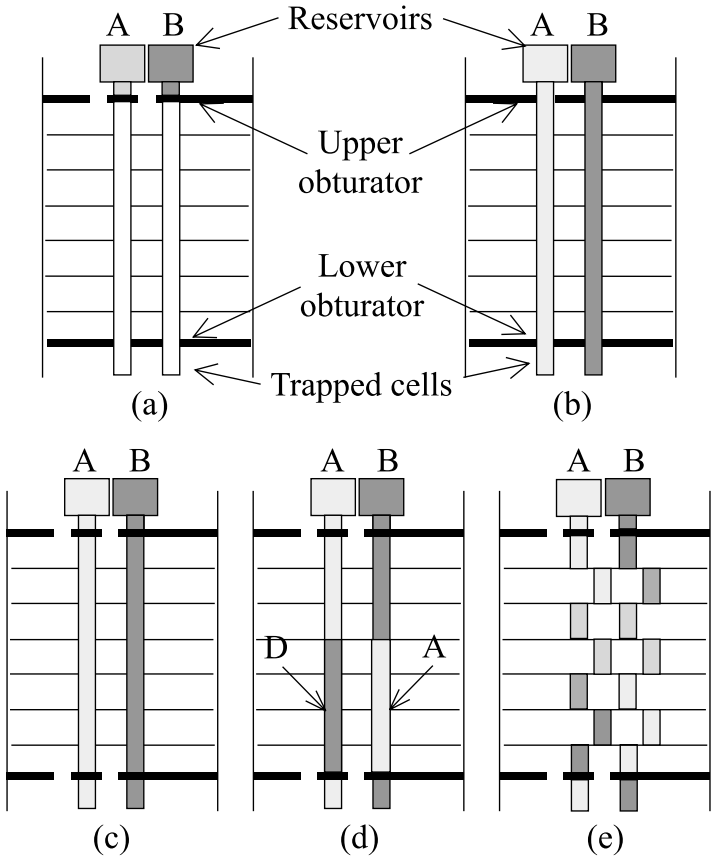

Fig. 3. Principle of our shear-cell: (a) melting; (b) filling; (c) isolation; (d) shearing; (e) contact.

At the end of the experiment, each segment is turned against its neighbour, isolating a small liquid element. The experiment is then cooled down and the composition of each piece of solid metal is determined by chemical analysis. The interest of this technique compared to the long capillary technique is that no quenching is needed to stop the experiment. It thus prevents segregation due to the solidification process which would change the initial concentration profile. Moreover, solid-state diffusion which could occur between the end of the experiment and chemical analysis is also cancelled. Another problem which may occur in shear cells is the misalignment of the segments constituting the capillary tubes, because of the mechanism taking a 100 μm wear. To get rid of this problem, a special pin (length 1000 mm, diameter 1.45 mm) is pushed through a small hole along the cell (diameter 1.5 mm) at each step from filling to shearing. Moreover, we have given a slight conicity (1% slope) to each segment of the capillary in order to make the extraction of the solid metal easier and to avoid breaking the pieces at each experiment. This conicity also ensures that the liquid metal surface in contact between two segments at each time remains the same even if any misalignment occurs.

Special attention must be given to the material of the tubes when working under a magnetic field. Usually, these are made up of graphite. But, because of thermoelectric effects, when two electrically conducting media are put together and if temperature or concentration gradients exist, a local current density appears [18]. Then the applied magnetic field creates a Lorentz force which pumps a new convection movement instead of braking it. This was observed by Mathiak et al. [19] who measured an apparent diffusion coefficient increasing with the applied field. In our experiment, the cells are thus made of a machinable ceramic (902 by Cotronics™). Because of the high friction coefficient of such a ceramic, it is compulsory to put a lubricant on the faces (Graphoil by Acheson™), in order to allow the shearing at the end of the experiment.

The whole cell is implemented in a specially designed furnace called experimental unit for research in diffusion influence of convection estimation (EURIDICE). Our

purpose is to accurately control the temperature gradients along the capillary tubes. The cell is thus put in a graphite cylinder (Fig. 4) which is heated by three heating elements. This cylinder is thermally insulated outside by a super-insulating material (Microtherm™) (thermal conductivity about 0.02 W/K/m). The first heating element compensates radial losses and the two other, at each end of the experiment, compensate axial losses. Thus, by regulating carefully the temperature of these three elements, it is possible to achieve a 0.1 K temperature uniformity along the capillary at 300°C. Temperatures are controlled by six thermocouples which can be moved along the graphite cylinder. A thermocouple can also be passed through the hole dedicated to the special pin mentioned above. At one end of the graphite cylinder, a metal ring is connected with the stainless steel outer envelope, to extract an axial heat flux. By symmetrically decreasing the temperature of the heating element at this end and increasing the temperature of the element at the other end of the graphite cylinder, an axial temperature gradient up to 200 K/m can be imposed. The whole experiment is insulated from external temperature perturbations by a water circulation around the external envelope. Temperature regulation of the experiment is insured by six PID processors (type 900 from Eurotherm™) implemented in a thermally controlled box. One is dedicated to the control of the ambient temperature in the box, one to the water cooled copper box in which are implemented the cold junctions of the thermocouples, one to water circulation around the external envelope and the three last ones to the three heating elements. We can thus expect a reliable control of the temperature during the experiments. The whole device is fixed on a vibration free support.

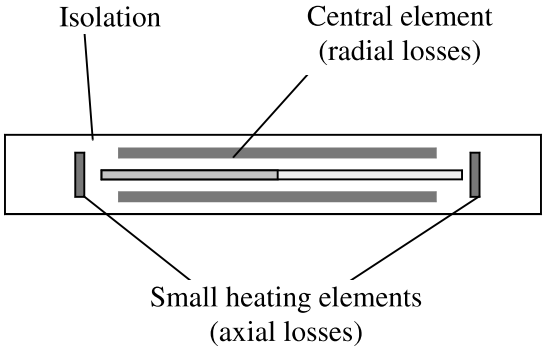

Fig. 4. Schematic of the EURIDICE cell.

The alloys processed in the experiment are prepared in a specially designed induction furnace. The melt is prepared and vigorously stirred by induction and injected in quartz crucibles (6 mm diameter, 1 m long) where it is quenched. One rod is enough for five experiments. Preparing large quantities allows to be more precise on the concentration of the initial melt (which is made by weighting). On the studied alloys, the remaining scattering of the concentration in the initial melt lies in the chemical analysis precision.

The magnetic field is created by an ordinary electromagnet. The field can reach a value of 0.75 T in a $10 \times 10 \times 40$ cm^3 volume. The values of the field in this volume has been controlled and a uniformity of 0.7% along the place where the capillaries are positioned has been observed.

At the end of the experiment, the 35 metal pieces of each capillary are analysed by inductively coupled plasma (ICP). The diffusion coefficient is deduced by a direct fit of the experimental data with an error function with a software written using Matlab™. Fig. 5 shows a typical experimental result. Several information help us to control that the samples have been processed correctly. The ICP analysis technique yields a 3% scattering on each measured concentration. It is thus checked that

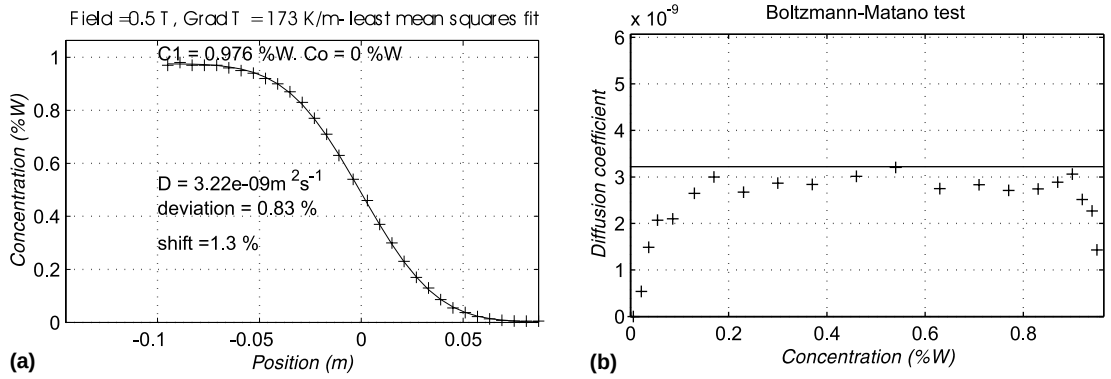

Fig. 5. A typical experimental result for Sn–SnIn(1%at.): experimental points (crosses) are fitted with an error function (full line). Note the rigourous erf-shape, though the measured coefficient is not the true diffusivity (2.6×10^{-9} m^2/s) because of convection.

Table 1
Experimental conditions and results

Composition	Mean temperature (°C)	Temperature gradient (K/m)	Field (T)	Duration (s)	$D_{app} \times 10^9$ (m^2/s)	Least mean squares deviation (%)	Offset (%)	Initial composition (%W)
SnIn(1%at.)	275	68	0.23	129 902	3.09	1.4	3.2	0.995
	275	68	0.23	129 902	2.8	1.2	0.29	1
	275	68	0.23	129 902	3.85	1.2	0.47	0.966
	275	68	0.23	129 902	3.66	0.94	1.2	0.94
	275	68	0.27	129 900	2.76	0.98	1.9	0.973
	275	68	0.27	129 900	3.3	0.95	1.1	0.978
	275	68	0.343	129 926	3	1.2	0.52	0.972
	275	68	0.343	129 926	2.71	0.88	0.25	0.983
	275	173	0.3	129 898	6.01	4.7	11	0.998
	275	173	0.35	129 907	4.31	0.97	1.2	0.97
	275	173	0.4	129 859	3.68	0.85	1.6	0.954
	275	173	0.4	129 859	3.77	0.99	1.1	0.958
	275	173	0.5	129 900	3.22	0.83	1.3	0.976
	275	173	0.75	129 875	2.69	1.3	1.6	0.981
	275	173	0.3	129 898	4.08	1.7		
	275	173	0.35	129 907	3.54	1.2	2.4	0.966
	275	173	0.4	129 859	3.31	1	1.9	0.921
	275	173	0.4	129 859	3.19	1.2	1.9	0.952
	275	173	0.5	129 900	2.79	0.76	0.84	0.983
	275	173	0.75	129 875	2.7	1.2	2.4	0.978
	250	68	0.25	26 189	2.31	4.3	0.71	0.99
	250	68	0.3	45 038	3.07	2.4	2.1	1.08
	250	68	0.4	92 688	2.3	1.9	1	1.06
	250	68	0.75	13 2912	2.2	3	1.9	1.07
	250	68	0.25	26 189	3.4	1.7	0.5	1.02
	250	68	0.3	45 038	2.53	2.7	3	1.08
	250	68	0.4	26 189	2.4	2	2.4	1.06
	250	68	0.75	13 2912	2.34	1.9	0.66	1.08
SnBi(0.5%at.)	275	0	0.4	93 564	7.27	2.3	0.36	0.975
	275	0	0.4	93 564	7.08	2.5	1.5	0.995
	275	0	0.45	93 685	6.23	2.1	0.15	0.982
	275	0	0.45	93 685	6.25	2.3	1.2	1
	275	0	0.5	93 642	5.52	2	0.68	0.954
	275	0	0.5	93 642	5.36	1.9	0.46	0.956
	275	0	0.6	93 614	4.31	2	0.98	0.972
	275	0	0.6	93 614	4.55	1.6	0.25	0.995
	275	0	0.75	93 590	3.53	1.3	1.9	0.979
	275	0	0.75	93 590	3.55	1.5	1.5	0.989
	275	0	0.5	46 800	7.11	2	0.49	0.991
	275	0	0.5	46 800	7.11	2.5	1.7	1.01
	275	0	0.5	71 491	5.93	2.3	1.2	0.975
	275	0	0.5	71 491	6.21	2.1	0.58	0.974

the standard deviation between the error function and the results remains in this range. Moreover, the symmetry of the experimental data with respect to the middle of the experiment is checked (still in the 3% range). Any experiment which does not follow these criterion is systematically rejected. At least, a Boltzmann–Matano [20] analysis is performed. Based on the properties of the error function, it gives the value of the diffusion coefficient at the point of the experiment where the concentration is C_1:

$$D_{C=C_1} = -\frac{1}{2t}\frac{\partial x}{\partial C}\int_0^{C_1} x\,\mathrm{d}C, \tag{17}$$

where $x(C)$ being the inverted concentration profile. Because of the chemical analysis scattering, the derivative $\partial x/\partial C$ is calculated by a second-order scheme di-

rectly on the measurements. This allows to check if the diffusion coefficient remains constant along the capillary, for example in the case of diffusion between two alloys showing a large concentration difference. In our case, only the central part is relevant: at the ends of the capillary, the slow variations of the concentration coupled with the chemical analysis scattering does not enable such an analysis ($\partial x/\partial C$ becomes infinite). In the central part of the capillary, the measured value is supposed to remain almost constant which shows the experiment has been performed correctly.

4. Experimental results: does a magnetic field modify atomic transport?

We performed 28 experiments on the Sn–SnIn(1%at.) couple and 14 experiments on the Sn–SnBi(0.5%at.) couple. All the results are presented in Table 1. Each couple shows a different behaviour concerning convective effects. In the case of Sn–SnIn(1%at.), the density difference between the two melts is extremely low ($\beta_c = 10^{-2}$) (see Table 2). We can thus study the influence of thermal convection on the measurements and two different temperature gradients (68 and 173 K m^{-1}) have been applied along the capillary. These temperature gradients are weak enough so the variations of the diffusion coefficient with temperature can be neglected. We here expect to be in the B^{-4} regime described previously. On the contrary, in the Sn–SnBi(0.5%at.) system, solutal effects are one order of magnitude stronger ($\beta_c = 0.3$). Experiments were performed in the isothermal configuration in order to study the behaviour of the measured diffusion coefficient with solutal convection (B^{-2} phase). In both cases, the applied magnetic field ranged between 0.2 and 0.75 T.

The results obtained on the tin–indium system are plotted on Fig. 6(a)–(c). At 250°C (average temperature), the asymptotic value is found to be 2.2×10^{-9} m^2 s^{-1} and at 275°C, 2.6×10^{-9} m^2 s^{-1}. Those values agree within the range of experimental scattering with previous experiments performed by Frohberg et al. [21] in microgravity on the tin–indium system. Because of the small diameter of the capillary, the Hartmann number is about 55 at 0.75 T. The variations of the coefficient α from expression (13) must be taken into account (see part I): we use the scale $\alpha(B)/B^4$ (the variations of α with the field are plotted in Part I, Fig. 3 [11]). It appears clearly that the measured diffusion coefficient decreases linearly with the magnetic field as $\alpha(B)/B^4$ on the x-axis. But, the experimental results separate into two straight lines. This is due to residual solutal effects. As mentioned previously (Section 3), because of the filling system of the capillaries, two capillaries have the Indium rich side (which is lighter) on the left-hand side while two capillaries have it on the right-hand side. But the temperature gradient is always applied in the same direction. So, in two capillaries, solutal and thermal buoyancy forces oppose each other (case $S < 0$ in expression (13)) while in the other, these buoyancy forces have the same direction (case $S > 0$). In the first case, the net transport by convection is reduced and in the other it is enhanced. Thus, even if the first B^{-2} phase is very short in this experiments (about 3 h), it leaves a memory on the final result. Eq. (13) was solved numerically with a direct first-order explicit scheme and is found to agree fairly well with experimental results with both an applied temperature gradient of 68 and 173 K/m. The analytical expression without the solutal contribution (Eq. (6)) lies between the two straight lines. The predicted slope is 0.33×10^{-9} USI with a temperature gradient of 68 K/m, the slopes found experimentally are 0.24×10^{-9} and 0.73×10^{-9} USI. With 173 K/m, the theoretical prediction is 2.11×10^{-9} USI and the experimental slopes are 2.07×10^{-9} and 3.69×10^{-9} USI. *It is thus clear that the only effect of the magnetic field is to damp natural convection and no effect on atomic transport can be detected in this range of field.* No evidence for some Marangoni convection due to a bad wetting of the liquid metal on the capillary has been found. At least, the scattering of the different results remains in a range of about 8%. Notice that all the results obtained on this device in this configuration are plotted here, except those showing clearly a failure (due to generally a bad mixing of the initial melt). From these results, we claim that the 30% scattering observed by other authors is due to uncontrolled convection in their experimental devices.

In the case of the Sn–SnBi(0.5%at.) couple, because of the higher solutal expansion coefficient, the experimental profile should not be an error function any more. However, the Maclean–Alboussière function described in Part I is so close to an error function that we performed the same fit as previously: no significant deviation from the error function fit can be observed in Fig. 7(a) (a direct fit with the real function does not give a significantly lower deviation). But the result of the Boltzmann–Matano analysis has here a parabolic aspect (Fig. 7(b)), while it is quite flat in Fig. 5 with Tin–Indium. To provide a comparison with this result, we performed this analysis on the theoretical function

Table 2
Numerical data

	SnIn(1%at.)	SnBi(0.5%at.)
σ	2.1×10^6 Ω^{-1} m^{-1}	2.1×10^6 Ω^{-1} m^{-1}
ρ	6.9×10^3 kg/m^3	6.9×10^3 kg/m^3
ν	2.3×10^{-7} m^2/s	2.3×10^{-7} m^2/s
β_c	2.2×10^{-2}	0.3
β_t	1.03×10^{-4}	9.5×10^{-5}[a]

[a] See Berthou and Tougas [22].

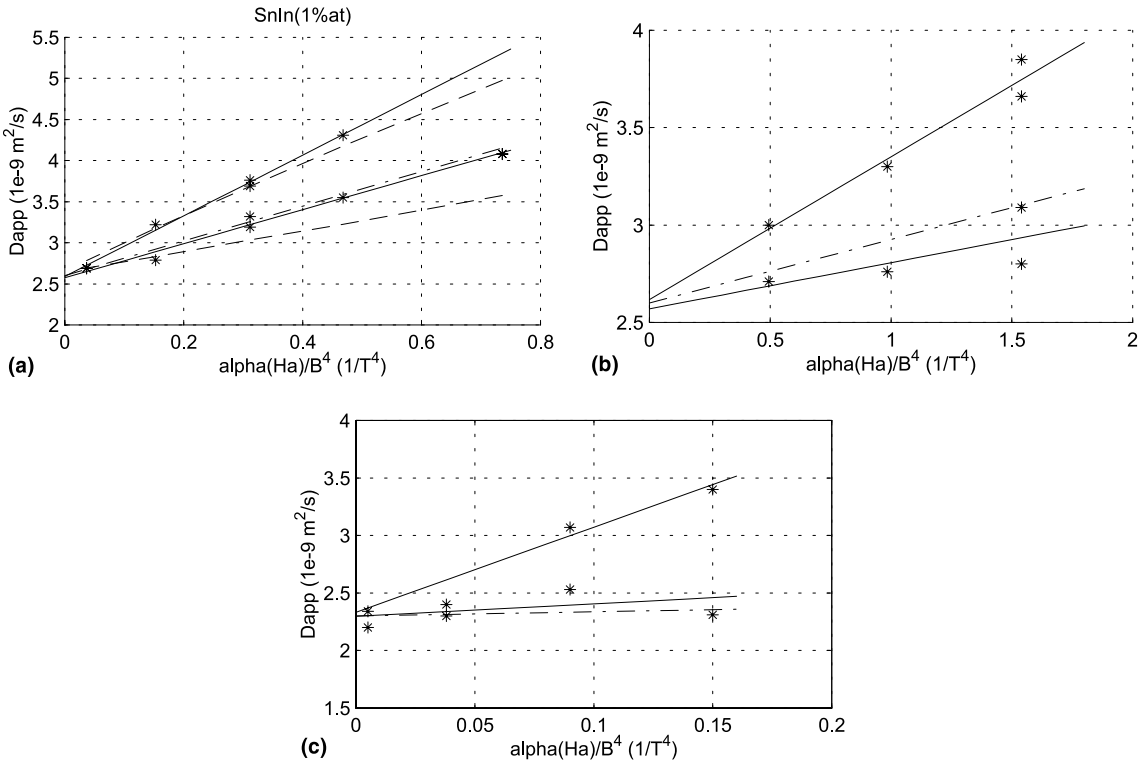

Fig. 6. Experimental results for Sn–SnIn(1%at.). Full lines: linear fits of experimental points (stars); dashed: 1D numerics; dash–dotted: theoretical prediction with no solutal convection. (a) 275°C mean temperature, 173 K/m temperature gradient, linear fits are: $D_{app} \times 10^9 = 2.59 + 3.69\,\alpha/B^4$ and $D_{app} \times 10^9 = 2.575 + 2.07\,\alpha/B^4$; (b) 275°C mean temperature, 68 K/m temperature gradient, linear fits are: $D_{app} \times 10^9 = 2.62 + 0.73\,\alpha/B^4$ and $D_{app} \times 10^9 = 2.57 + 0.24\,\alpha/B^4$; (c) 250°C mean temperature, 68 K/m temperature gradient, linear fits are: $D_{app} \times 10^9 = 2.33 + 7.39\,\alpha/B^4$ and $D_{app} \times 10^9 = 2.30 + 1.08\,\alpha/B^4$.

(Fig. 7(c)). The same parabolic shape is found. It can thus be stated that, even if the experimental result still looks like an error function, it might actually follow the Maclean–Alboussière function. The results obtained on the Sn–SnBi(0.5%at.) are plotted on Fig. 8(a) as a function of $1/B^2$. A good agreement with the theoretical predictions is found again. No influence of the magnetic field can neither be detected. However the field is not high enough to sufficiently damp solutal convection out: the asymptotic value of the measured diffusion coefficient is not reached. An extrapolation made with the results of numerical simulation of Eq. (13) yields an impurity diffusion coefficient between 2.1 and 2.5×10^{-9} m^2 s^{-1}. No microgravity experiment is available yet to allow comparisons. In Section 2, we point out that in the case of solutal convection, the measured diffusion coefficient also depends on the duration of the experiment. We performed four experiments with the same applied magnetic field, but with different duration (see Fig. 8(b)). We found that the measured diffusion coefficient follows a $\tau^{-0.4}$ law, which is very close to the predicted $\tau^{-1/2}$ law. This variation of the measurement with time might perhaps also be one of the reasons for experimental scattering in previous diffusion experiments.

5. Conclusion: can the magnetic field be an alternative to microgravity?

Up to now, the only reliable impurity diffusion coefficient measurements have been performed under microgravity conditions to avoid buoyancy driven convection. Our purpose was to show that it is possible to make reliable ground-based experiments, using an uniform magnetic field to damp the liquid metal flow. The first step is to theoretically quantify the influence of the fluid flow on the measured diffusion coefficient. The effect of MHD braking can then be taken into account. We have shown that two regimes should be distinguished:

- When thermal convection is predominant, the evolution of the average concentration profile follows a diffusive law with a modified (constant) diffusion co-

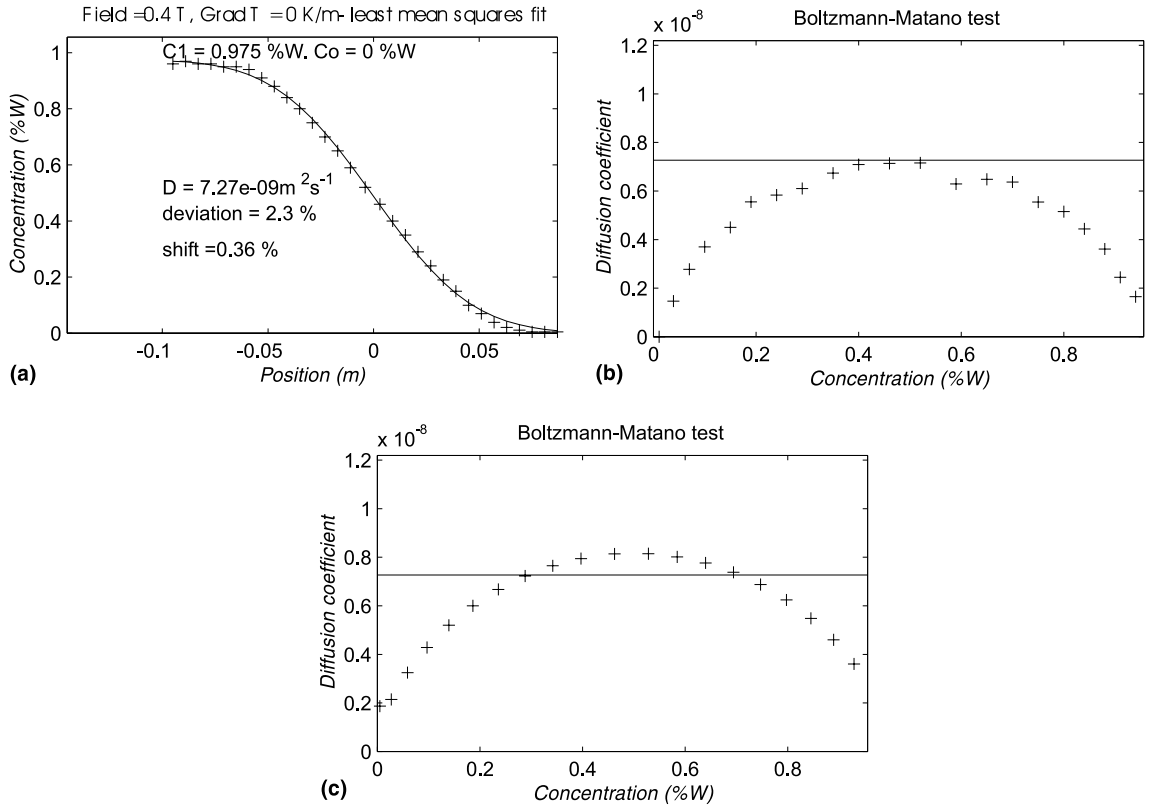

Fig. 7. Typical result for the Sn–SnBi(0.5%at.) couple. (a) experimental points (crosses) fitted with an error function; (b) experimental Boltzmann–Matano test; (c) theoretical Boltzmann–Matano test on the Maclean–Alboussière function.

efficient. This apparent diffusion coefficient decreases as B^{-4} with the applied magnetic field.

- When solutal convection is predominant, the apparent diffusion coefficient depends on the duration of the experiment and decreases as B^{-2}. The concentration profile does no longer follow a diffusive law, but still 'looks like it'.

To assess these theoretical considerations, a convection controlled shear cell was built. In this device, the temperature profile is carefully controlled along the capillaries as well as the position of the cell's segments during operation. Special attention is also given to the composition of the initial melt to ensure reproducible

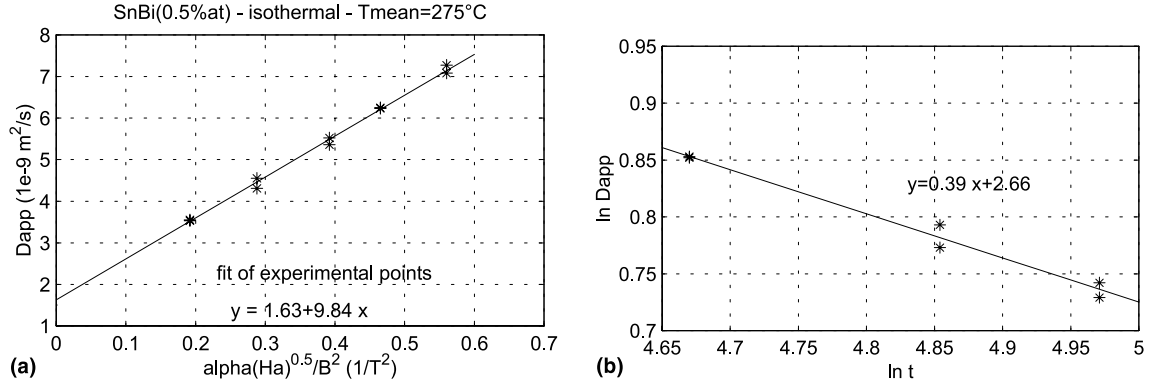

Fig. 8. Experimental results for Sn–SnBi(0.5%at) at 275°C, isothermal: (a) measured diffusivities, varying the magnetic field, fixed duration of experiments; (b) measured diffusivities, fixed field (0.5 T), varying duration of experiments.

solutal convection. Different magnetic fields up to 0.75 T were then applied.

The experiments were performed on the Sn–SnIn(1%at.) diffusion couple with an applied temperature gradient to check the braking of thermal convection and on the Sn–SnBi(0.5%at.) couple in an isothermal configuration to show the effect of solutal convection. A good agreement (in the range of experimental scattering i.e. 8%) is found with previous microgravity experiments on the Sn–SnIn couple. All the results agree with the theoretical damping laws for the influence of the magnetic field on both couples with an accuracy in the range of experimental scattering due to chemical analysis. Thus, the important scattering reported by previous authors in such measurements may be due to uncontrolled convection. At least, no influence of the magnetic field on atomic transport is detected: the only measurable effect of the field is the damping of natural convection.

These first results show that the use of a magnetic field to measure impurity diffusion coefficients is a promising method, provided the initial convection (thermal and solutal) is well controlled. The MHD damping laws can then be checked: a deviation from these laws would show an influence of the field on atomic transport and only microgravity measurements would then be possible. In the case of solutal convection which is encountered most often in such measurements, a 0.75 T magnetic field is too low. Calculations show that a field around 2.5 T would be enough to measure most of the diffusion couples in liquid metals (excepted very high density differences coupled with a very low diffusion coefficient). Such a field is high, but quite common nowadays (Mathiak et al. [19] used a 10 T field). A new set of experiments has to be performed in this range of high magnetic fields and compared with other microgravity results. If still no influence of the field is detected, this method would then be a fast, reliable and cheap technique to measure diffusion coefficients even in the case of technical multi-constituted alloys.

Acknowledgements

This work is financially supported by the national French space agency (CNES). Thanks to Pr Zappoli from CNES for his confidence in our work. Special thanks to Dr. Jean-Paul Garandet who initiated this program, for all the fruitful discussions about the topic. We are also very grateful to M. Duteil from the Centre of Chemical Analysis of the CNRS in Solaize (France) for the high quality of his chemical analysis. A special mention to Pr Muller-Vogt who pointed out to us all the problems of diffusion coefficient measurements and whose team performed the first chemical analysis for us.

References

[1] W. Kurz, D.J. Fisher, In Fundamentals of Solidification, Trans Tech Publications, 1989.
[2] J.P. Praisey, Benefits of microgravity for measuring thermotransport coefficients in liquid metallic alloys, Int. J. Heat Mass Transfer 32 (12) (1989) 2385–2401.
[3] G. Müller-Vogt, R. Kössler, Application of the shear cell technique to diffusivity measurements in melts of semiconducting compounds: Ga–Sb, J. Cryst. Growth 186 (1998) 511–519.
[4] J.I.D. Alexander, J.F. Ramus, F. Rosenberger, Numerical simulations of convective contamination of diffusivity measurements in liquids, Microgravity Sci. Technol. 9 (1996) 158.
[5] A. Bejan, C.L. Tien, Laminar natural convection heat transfer in a horizontal cavity with different end temperatures, J. Heat Transfer 100 (1978) 641–647.
[6] J.P. Foster, R.J. Reynik, Self diffusion in liquid tin and indium over extensive temperature ranges, Met. Trans. A 4 (1973) 207–216.
[7] G. Mo, F. Rosenberger, Molecular-dynamics simulation of flow with binary diffusion in a two-dimensionnal channel with atomically rough walls, Phys. Rev. A 44 (1991) 4978.
[8] T. Alboussière, J.P. Garandet, R. Moreau, Asymptotic analysis and symmetry in MHD convection, Phys. Fluids 8 (8) (1996) 2215–2226.
[9] W.V. Youdelis, R.C. Dorward, Directional solidification of aluminium–copper alloys in a magnetic field, Can. J. Phys. 44 (1966) 139–150.
[10] W.V. Youdelis, J.R. Cahoon, Diffusion in a magnetic field, Can. J. Phys. 48 (1970) 905–908.
[11] D.J. Maclean, T. Alboussière, Measurement of solute diffusivities. Part I. Analysis of coupled solute buoyancy-driven convection and mass transport, Int. J. Heat. Mass Transfer 44 (9) (2001) 1639–1648.
[12] J.P. Garandet, T. Alboussière, R. Moreau, Buoyancy driven convection in a rectangular enclosure with a transverse magnetic field, Int. J. Heat Mass Transfer 35 (4) (1992) 741–748.
[13] L. Davoust, R. Moreau, A.C. Neubrand, R. Bolcato, Experimental results on MHD free convection in a horizontal cylinder, in: H. Branover, Y. Unger (Eds.), Progress in Fluid Flow Research: Turbulence and Applied MHD, American Institute of Aeronautics and Astronautics, 1998 (Chapter 49).
[14] G. Taylor, Dispersion of soluble matter in solvent flowing slowly through a tube, Proc. Roy. Soc. London A 219 (1953) 186–203.
[15] T. Alboussière, J.P. Garandet, P. Lehmann, R. Moreau, Convective effects in the measurement of diffusivities and thermotransport coefficients. Liquid metal alloys and the use of a magnetic field, Entropie 218 (1999) 59–62.
[16] R. Moreau, in: Magnetohydrodynamics, Kluwer Academic Publishers, Dordrecht, 1990.

[17] M.D. Cowley, On the temperature distribution due to convection in the horizontal Bridgman crystal growth configuration with vertical magnetic field, Proceedings of the Second International Conference on Energy Transfer in Magnetohydrodynamic Flows, Aussois, 1994, pp. 27–36.
[18] P. Lehmann, R. Moreau, D. Camel, R. Bolcato, Modification of interdendritic convection in directional solidification by a uniform magnetic field, Acta Mater. 46 (11) (1998) 4067–4079.
[19] G. Mathiak, A. Griesche, G. Frohberg, Diffusion in liquid metals, in: 9th European Symposium on Gravity Dependent Phenomena, Berlin, 1995.
[20] J. Crank, The Mathematics of Diffusion, Clarendon Press, Oxford, 1956, p. 148.
[21] G. Frohberg, H. Kraatz, H. Wever, A. Lodding, H. Odelius, Diffusion in liquid metals: self and impurity diffusion, Defect Diff. Forum 66–69 (1989) 295–300.
[22] P.E. Berthou, R. Tougas, The densities of liquid In–Bi, Sn–In, Bi–Sb and Bi–Cd–Ti alloys, Metall. Trans. 1 (1970) 2978.
[23] C. Barat, J.P. Garandet, The effect of natural convection in liquid phase mass transport coefficient measurements: the case of thermosolutal convection, Int. J. Heat Mass Transfer 39 (10) (1996) 2177–2182.